Process modelling and simulation for continuous pharmaceutical manufacturing of artemisinin

Process modelling and simulation for continuous pharmaceutical manufacturing of artemisinin

Hikaru G. Jolliffe and Dimitrios I. Gerogiorgis*

Institute for Materials and Processes (IMP), School of Engineering, University of Edinburgh, The King's Buildings, Edinburgh, EH9 3JL, United Kingdom

**Corresponding author: D.Gerogiorgis@ed.ac.uk (+44 131 6517072)*

ABSTRACT

Recent advances in pharmaceutical manufacturing techniques are showing the promise of continuous production, and pharmaceutical firms, currently reliant on mature batch technology, are beginning to turn toward Continuous Pharmaceutical Manufacturing (CPM). Continuous production techniques have efficiency, cost, reliability and quality advantages: in this paper we evaluate and quantify these for the case of the CPM of artemisinin, a key antimalarial Active Pharmaceutical Ingredient (API). Published reaction and unit operation data are analysed, static models developed, and continuous plug flow reactors designed for a reference case producing 100 kg of API per year: the small reactor volumes computed (19.72 mL and 78.72 mL) illustrate one benefit of continuous techniques, that of small equipment footprint. In addition, alternative CPM cases are also computed whereby different continuous API recovery operations are evaluated in comparison to the base case; the latter employs a reported batch product recovery. Utilising published solubility data as well as data estimated using the UNIFAC method, systematic evaluation identifies ethanol (EtOH) and ethyl acetate (EtOAc) as good candidate anti-solvents for continuous crystallisation. For the same 100 kg per year production level of API, designs using continuous separation techniques can achieve significantly improved E-factor values (22.52 average) compared to the batch process (65.28), implying enhanced sustainability through reduced waste generation. This API of critical societal importance is a good candidate for CPM, with the future benefits of performing full analysis and technoeconomic optimisation evident.

Highlights:

- Historic analysis of artemisinin price, production and market demand.
- Novel kinetic data analysis and reactor design for complex organic reactions in flow.
- Systematic evaluation of antisolvents for continuous product separation schemes.
- Ethanol and ethyl acetate emerge as good candidates for continuous crystallisation.
- Continuous designs generate 66.2% less waste (lower E-factors) than reference batch case.

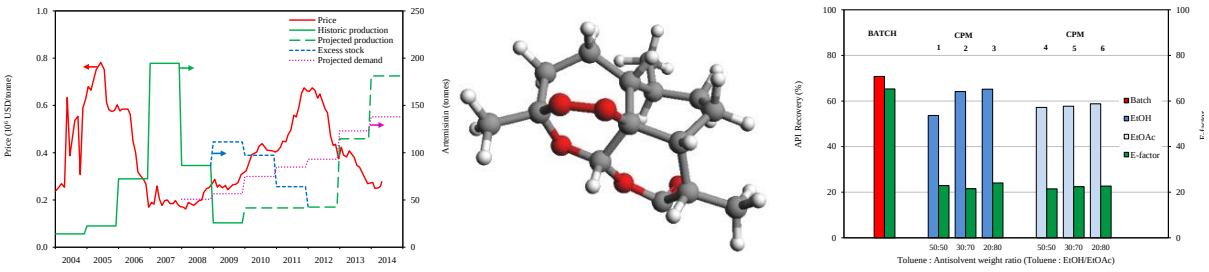

1 INTRODUCTION

Driven by market and technological drivers including increasing R&D costs and competition from generic manufacturers (Behr et al., 2004; Jolliffe and Gerogiorgis, 2015a), the paradigm of batch manufacturing, the predominant method of pharmaceutical production, is being challenged by recent work in the field of Continuous Pharmaceutical Manufacturing (CPM) which has gained support at the highest regulatory levels (Plumb, 2005; Lee et al., 2015). Batch process efficiency can be very low, with high rates of waste production and solvent use, while inherently poor heat and mass transfer lead to difficulties in process scale-up (Anderson, 2012; Gernaey et al., 2012). In contrast, continuous production methods offer higher yields, smaller equipment, more efficient solvent and energy use, and safer, more reliable operation (Roberge et al., 2008; Anderson, 2012); industries such as the petrochemicals sector have benefited from the advantages of continuous processing for many years (Schaber et al., 2011).

Investigating the feasibility and viability of CPM processes via process modelling and simulation is a rapid and cost-efficient methodology which can be used to quantitatively evaluate the benefit and potential of continuous processes for pharmaceutical production (Gerogiorgis and Ydstie, 2005; Gerogiorgis and Barton, 2009; Teoh et al., 2015); furthermore, elaborate design and optimisation of multiphase unit operations are also possible, given the vast computational power and robust software now available for high-fidelity simulations (Gerogiorgis and Ydstie, 2003; Gerogiorgis et al., 2003). High-resolution model-based control studies thus advance the state of the art (Nayhouse et al., 2015).

We have previously shown how systematic analysis can identify good candidates for CPM, and have performed initial technoeconomic comparisons of the CPM of two key Active Pharmaceutical Ingredients (API), ibuprofen and artemisinin (**1**) (Jolliffe and Gerogiorgis, 2015a, 2015b). Here, we present in detail a more in-depth model and steady state simulation of the continuous production of artemisinin, one of the most effective anti-malarial APIs available today. The flowsheet used is adapted from published continuous chemical synthesis routes, the kinetics of which have been analysed and used for systematic reactor design (Kopetzki et al., 2013).

Malaria is a disease of extreme importance. There are an estimated 225 to 500 million annual cases of malaria from *Plasmodium falciparum* (the main strain of malaria-causing parasite), resulting in approximately one million deaths, while *P. vivax* (a strain causing marginally more benign but still potentially fatal symptoms) causes 70 to 390 million cases a year. It disproportionately affects low-

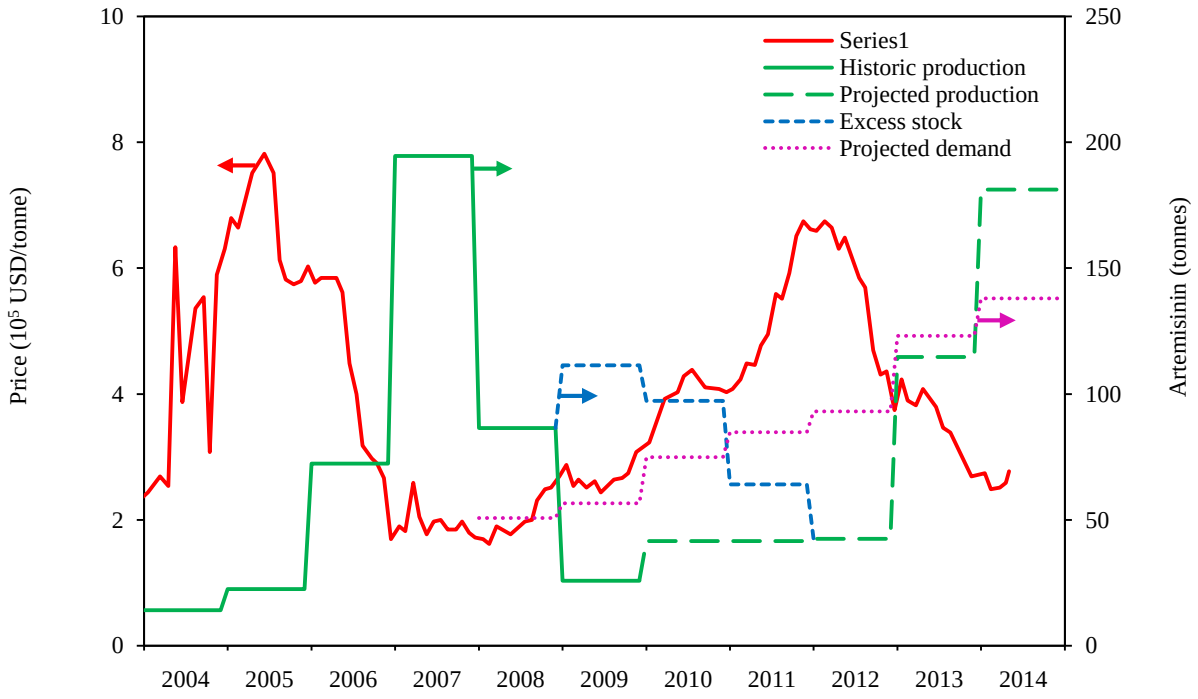

Fig. 1. Historic and projected artemisinin market data (The Boston Consulting Group, 2009; Bionexx, 2014).

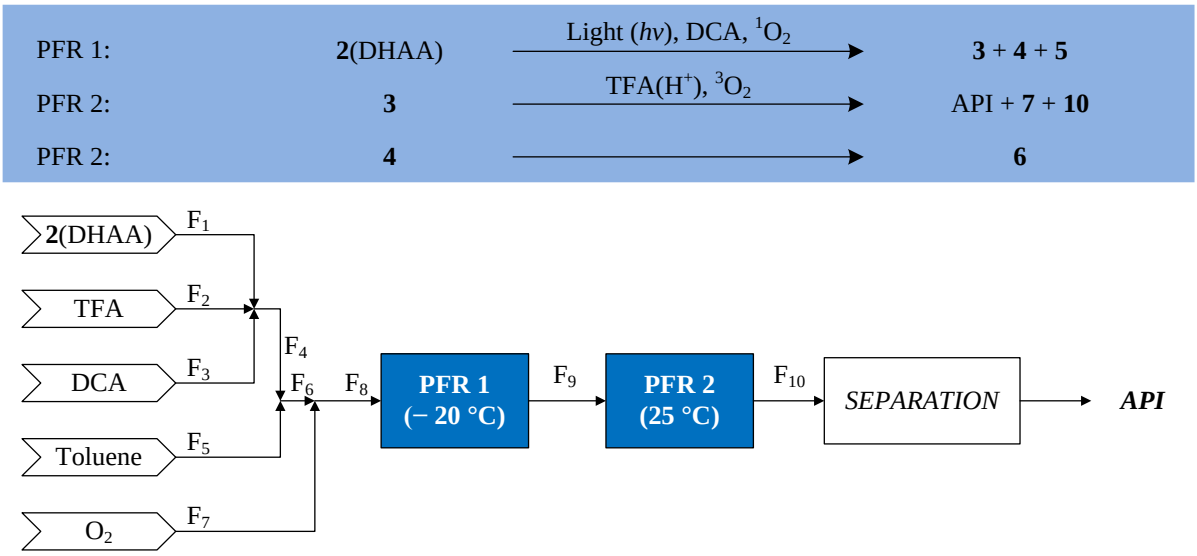

Fig. 2. Conceptual flowsheet for continuous production of artemisinin (adapted from Kopetzki et al., 2013).

income regions and young children, and has significant detrimental effects on economies through lost productivity (Davis et al., 2011). Present mainly in tropical regions, it can be found in Central and South America, large areas of Asia and Africa, the Caribbean, and the Middle East.

Artemisinin and its medicinal and therapeutic properties (White, 2008) have long been known: the natural source of artemisinin, the plant sweet wormwood (*Artemisia annua*), has featured in traditional Chinese medicine for at least two millennia, and an early reference to its use in treating malaria can be found in a medical text from 1596 (Tu, 2011; Henry, 2014). Known in Chinese as *qinghao*, artemisinin was first isolated and identified as a result of a project to find cures and treatments for malaria (Tu et al., 1981; Tu et al., 1982). The *2015 Nobel Prize in Physiology or Medicine* was awarded to Youyou Tu for her discovery of artemisinin (The Nobel Assembly, 2015).

Artemisia annua is native to temperate regions of Asia, but can now be found in various other locations with suitable climactic conditions; main cultivation and production centres are China (180-200 tonnes of artemisinin in 2011), Vietnam (23-26 tonnes), Madagascar (16 tonnes were projected for 2013) and East Africa (Kenya and Uganda, 14 tonnes projected for 2013) (Cutler, 2013). Other minor producers include India, Australia, Papua New Guinea, West Africa, Brazil, Argentina, UK, USA, and Switzerland (Ellmann, 2010). Current production methods are predominantly plant cultivation and subsequent batch extraction, a process which has long lead times between 12−14 months (seed planting to API extraction) (Hommel, 2008). In conjunction with the fluctuating and unpredictable artemisinin demand (e.g. malaria is transmitted by mosquitos, the levels of which can be significantly affected by weather) this leads to highly variable prices: from 2007 to 2011 it was between $200-$400 per kilogram, rising to $900 at the end of 2011 (due to shortages from poor harvests) before dropping again to $400 in 2012, and to $360 at the start of 2013 (Cutler, 2013). Indeed, comparisons of global monthly artemisinin prices and production levels illustrate periods of over production (2007, 2014) caused by price peaks several years prior (2005, 2012) (Fig. 1).

In anti-malaria medications, artemisinin derivatives are often used to enhance bioavailability, and these are often used in conjunction with other antimalarial substances in Artemisinin Combination Therapies (ACT), and it is these which constitute the majority of formulations that are sold. The artemisinin derivative targets the bulk of the parasitic infection within the first three days, with the partner substance targeting residual parasite levels (World Health Organisation, 2015). Examples of derivatives include artesunate (water-soluble), artemether (lipid-soluble) and artemotil (Miller and Su, 2011), while partner anti-malarial substances they are often combined with include lumefantrine, amodiaquine, mefloquine, piperaquine and pyronaridine. The range of subtances available is also beneficial in delaying the onset of resistance of the parasites to the medication.

The Global Fund reports that, in the 2008 to 2014 period, the anti-malarial market was worth $340 million with two categories of ACTs – artemether-lumefantrine (AL) and artesunate-amodiaquine

(ASAQ) – collectively constituting 87% of this. There are five main pharmaceutical firms involved: Novartis and Ajanta producing AL, Sanofi Aventis producing ASAQ, and Ipca and Cipla producing both forms (Bionexx, 2014).

Demand for ACTs can be highly variable (The Boston Consulting Group, 2009), and although artemisinin price fluctuations have an impact on the costs to firms producing ACTs, due to the moderately low impact of artemisinin value on the ACT selling price. For eight major ACT formulations (four AL, four ASAQ), constituting 354 million treatments at 292 million USD (average ACT price 0.82 USD per dose), artemisinin constituted between 20-23% of cost for AL formulations and between 10-29% for ASAQ formulations, an average of 21%, minimizing somewhat the cost to end purchasers (Bionexx, 2014).

In recent years, there have been attempts to produce synthetic (Zhu and Cook, 2012) and semi-synthetic (Paddon et al., 2013; Peplow, 2013; Paddon and Keasling, 2014; Turconi et al., 2014) artemisinin by a variety of methods in order to stabilise production levels, including the use of biotechnology (Hommel, 2008; Wang et al., 2014; Abdin and Alam, 2015; Corsello and Garg, 2015). Of particular interest is the recent demonstration of the continuous synthesis for this key pharmaceutical from the waste material from one of the current batch extraction processes (Lévesque and Seeberger, 2012; Kopetzki et al., 2013). Dihydroartemisinic acid (DHAA, **2**) is normally discarded as waste: in the process developed by Kopetzki et al., (2013), on which this work is based, photo-oxidation with the subsequent use of acid catalyst is used to transform **2** via several intermediates to artemisinin. Further developments of this process have been reported to produce various artemisinin derivatives, and there are plans to commercialise the process (Extance, 2012; Gilmore et al., 2014; Seeberger et al., 2014). Other groups are also pursuing similar routes: strategies applying Green Chemistry principles to continuous artemisinin synthesis involving liquid CO_2 solvent with catalysts, as well as synthesis using benign, simple solvents (ethanol and water), are being explored (Amara et al., 2015).

Product recovery and crystallisation is a well-established operation, and is used in many industries, in both batch and continuous operation; the latter is predominantly used for the largest scale processes (Ward et al., 2011). In recent years, there have been advances in the study of the continuous crystallisation of APIs using both well-mixed (Kwon et al., 2014a) and plug-flow (Kwon et al.,

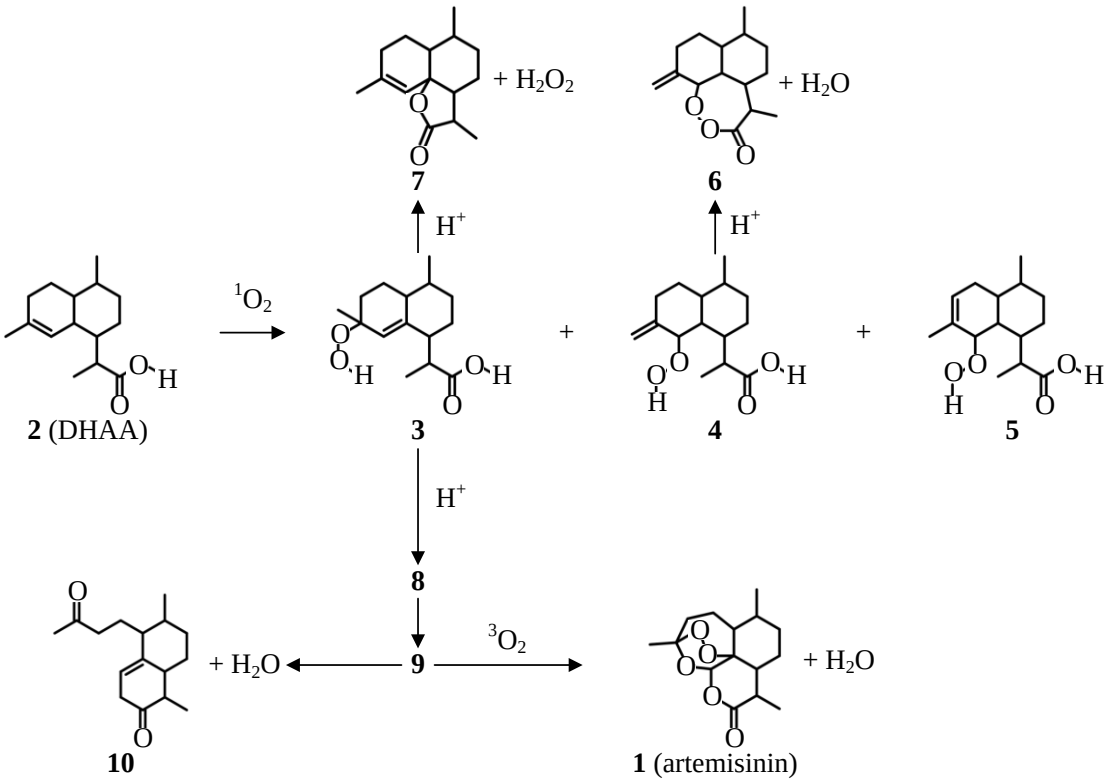

Fig. 3. Reaction scheme detailing synthesis path from feed material **2** to product API **1** and side products via intermediates (Kopetzki et al., 2013).

Table 1. Main component molar and mass flow changes due to all three continuous flow reactions.

Component	Stoichiometric coefficient	Selectivity (%)	Flow in (mmol hr^{-1})	Flow in (g hr^{-1})	Flow change (mmol hr^{-1})	Flow change (g hr^{-1})	Flow out (mmol hr^{-1})	Flow out (g hr^{-1})
PFR 1								
2 (DHAA)	−1		98.59	23.30	−96.62	−22.84	1.97	0.47
O_2	−1		318.18	10.18	−96.62	−3.09	221.56	7.09
3	+1	86.6[a]	0	0	+83.67	+22.45	83.67	22.45
4	+1	10.3[a]	0	0	+9.96	+2.67	9.96	2.67
5	+1	3.1[a]	0	0	+2.99	+0.80	2.99	0.80
PFR 2								
2 (DHAA)	−	−	1.97	0.47	−	−	1.97	0.47
O_2	−1	−	221.56	7.09	−62.56	−2.00	158.99	5.09
3	−1	−	83.67	22.45	−69.87	−18.75	13.81	3.70
4	−1	−	9.96	2.67	−6.10	−1.64	3.86	1.04
5	−	−	2.99	0.80	−	−	2.99	0.80
6	+1	100.0[c]	0	0	+6.10	+1.53	6.10	1.53
7	+1	6.7[b]	0	0	+4.66	+1.09	4.66	1.09
10	+1	3.8[b]	0	0	+2.65	+0.66	2.65	0.66
1(API)	+1	89.5[b]	0	0	+62.56	+17.66	62.56	17.66

2014b) crystallisers. Although few in number at this stage, there have been demonstrations of continuous API crystallisation in pilot plants (Zhang et al., 2014).

Process control in continuous pharmaceutical operations is of course of paramount importance. For continuous crystallisation control key process parameters include crystal size and shape, and toward this process modelling has been frequently successful (Griffin et al., 2010; Kwon et al., 2013). Very recently, implemented (i.e. model-free) plantwide control for a CPM process has been demonstrated, also incorporating crystallisation (Lakerveld et al., 2014). The modelling and control of a novel dropwise additive manufacturing process for pharmaceutical products (DAMPP) has also been reported (Içten et al., 2015).

This paper is organized in the following manner: first, the process flowsheets and reactions are

Table 2. Process mass balance (g hr^{-1}).

	Stream									
Component	**F_1**	**F_2**	**F_3**	**F_4**	**F_5**	**F_6**	**F_7**	**F_8**	**F_9**	**F_{10}**
2 (DHAA)	23.30	0	0	23.30	0	23.30	0	23.30	0.47	0.47
1 (API)	0	0	0	0	0	0	0	0	0	17.66
DCA	0	0.11	0	0.11	0	0.11	0	0.11	0.11	0.11
TFA	0	0	5.62	5.62	0	5.62	0	5.62	5.62	5.62
O_2	0	0	0	0	0	0	10.18	10.18	7.09	5.09
3	0	0	0	0	0	0	0	0	22.45	3.70
4	0	0	0	0	0	0	0	0	2.67	1.04
5	0	0	0	0	0	0	0	0	0.80	0.80
6	0	0	0	0	0	0	0	0	0	1.53
7	0	0	0	0	0	0	0	0	0	1.09
10	0	0	0	0	0	0	0	0	0	0.66
H_2O_2	0	0	0	0	0	0	0	0	0	0.16
H_2O	0	0	0	0	0	0	0	0	0	1.28
Toluene	0	0	0	0	168.27	168.27	0	168.27	168.27	168.27
Total	23.30	0.11	5.62	29.04	168.27	197.30	10.18	207.48	207.48	207.48

introduced, before kinetic data analysis and parameter estimation is covered along with process mass balances and plug flow reactor design methodology. The process for the design of continuous separations is given next, before results for mass balances, reactor designs and separations are evaluated in relation to typical performances for pharmaceutical processes. Detailed models for the calculation of API solubilities by the UNIFAC method are given in the Appendix.

2 FLOWSHEET AND PROCESS MODELLING

The flowsheet is based on a recent proven continuous synthesis route (Fig. 2) (Kopetzki et al., 2013). Artemisinin is produced in a series of two plug flow reactors, the first reactor being a chilled photo-oxidation reactor operating at −20°C. Here, raw material **2** (DHAA) is photo-oxidised (Shenck ene reaction) to key intermediate **3**. DCA (9,10-dicyanoanthracene) is a photosensitiser, essential to allow the production of the singlet oxygen necessary for the photooxidation reaction; light is provided by a suitable source such as a high-power mercury lamp (Kopetzki et al., 2013). Intermediate **4** and by-product **5** are also produced (Fig. 3).

Subsequently in PFR2, a variety of reactions and transformations occur. Intermediate **3** (with trifluoroacetic acid – TFA – acting as acid catalyst) produces side product **7** by proximal protonation; terminal protonation results in a Hock rearrangement leading to **9**, which in turn either transforms into byproduct **10** via isomerisation or reacts with triplet oxygen to produce the API artemisinin (**1**). Other minor byproducts include hydrogen peroxide (H_2O_2, the loss of which leads to **7**) and water (the loss of which leads to **6**, **10** and **1**) (Gilmore et al., 2013). A dehydrating cyclisation of **4** produces byproduct **6**; in some conditions, **5** may further react, but negligible amounts are present under the operating conditions studied here (Kopetzki et al., 2013).

PFR reactor design requires the calculation of the process mass balances (Table 1, Table 2). The starting point is a recent synthesis study (Kopetzki et al., 2013), with the following assumptions: 1) reactions occur only inside the PFR reactors and not in any of the lines connecting them, 2) isothermal operation is ensured in all reactors via suitable heating media, 3) temperature changes cause no phase transformation or precipitation affecting the flow, 4) reactions shown in Fig. 3 are the only ones which occur, 5) gas-to-liquid mass transfer in in the reactors is not limiting and does not impede the reactions in any way.

3 KINETIC PARAMETER ESTIMATION AND REACTOR DESIGN

The reactions for the CPM of artemisinin have been assumed to be first-order given the nature of the reactions (large organic molecules reacting with excess of smaller reagents, e.g. O_2); data was available for these reactions (Kopetzki et al., 2013; Seeberger et al., 2014). Kopetzki et al. (2013) employed pure oxygen supplied at 10 bar with a volumetric flow at the inlet of 5 mL min^{-1}, corresponding to 3.2 equivalents with respect to feed DHAA, reducing to 1.9 mL min^{-1} (at 10 bar) after all reactions are complete, implying a feed oxygen excess of 61.2%. Experimental measurements of oxygen solubility in toluene indicate saturated O_2 concentrations of 0.65% and 0.84% at −20°C and 25°C , respectively, at 10 bar (corresponding to Henry's constant values of 154.8 MPa and 118.4 MPa – determined from literature) (Li et al., 2007; Wu et al., 2014). Good mixing that is achievable with small process line and reactor dimensions, and high interfacial area (up to 25,300 m^2/m^3), can ensure that the reaction is not impeded and for a first-order assumption to hold (Seeberger et al., 2014).

Reaction rate constants have been estimated based on stated conversions and lab-scale reaction line volumes, with mathematical programming used to find rate constant values. Reciprocals of instantaneous reaction rates can be plotted against conversion, assuming a given value for the rate constant, and necessary reactor volumes can be determined from the area under the curve, as this corresponds to reactor volume over the product of volumetric flow and inlet reactant concentration. Nonlinear optimisation allows the determination of necessary values of the rate constant for calculated reactor volumes to match the experimental reactor volumes.

In the first PFR, the photo-oxidation reaction can achieve 98% conversion of **2** (DHAA), with product selectivities of 86.6% (**3**), 10.3% (**4**) and 3.1% (**5**) (Table 3), with the aforementioned kinetic data analysis implying a rate constant of 39.12 hr^{-1}; this is for the reaction conducted at −20°C (Kopetzki et al., 2013). This agrees well with additional data (Fig. 4A), with a value of 38.8 hr^{-1} for

the same reaction at −18°C (Table 4) (Seeberger et al., 2014). It can be seen that the rate constant has very non-monotonic behaviour and high variability with respect to temperature: this is as experimental data indicates highly variable non-monotonic conversions with respect to temperatre, although desired product selectivity is monotonic, increasing with decreasing temperature (see page 32, Table 4 in the publication of Seeberger et al. (2014)). The continuous line is a linear best fit of data with conversions explicitly given for different reaction times (see page 32, Table 3 in the publication of Seeberger et al. (2014)), with the rate constant (65.5 hr^{-1}) determined from the slope. An outlying data point at t = 0.051 hr (not shown) has been discounted: this fell significantly below the trend, implying higher reactant consumption than expected. A possible explanation is that the higher reaction time allowed sufficient temperature increases for higher conversions (cooling is required to maintain temperatures) (Seeberger et al., 2014).

For the dashed lines in Fig. 4A the rate constants have been determined using nonlinear optimisation. Although a different solvent (dichloromethane, DCM) and photosensitizer (tetraphenyl porphyrin, TPP) were used in these cases, similar yet better conversions and selectivities can be achieved using toluene and DCA, ensuring that the use of kinetic parameters determined from the DCM and TPP data will give marginally over-designed reactors (Seeberger et al., 2014).

For the second reaction (mutliple transformations beginning with intermediate **3** and resulting in **1**, artemisinin) a conversion has been calculated based on data for the reaction conducted in batch at small scale (5 mL total volume) for a duration of 20 minutes (Fig. 4B) (Kopetzki et al., 2013; Seeberger et al., 2014). The reported yields (based on the original quantity of **2**) of **1**, **7**, and **10** are 59.1%, 4.4%, and 2.5%, respectively. In conjunction with data for the conversion of **2** (DHAA) in the first PFR, a 78% conversion of **3** in the second PFR can be estimated from these values, with product selectivities of 89.5%, 6.7%, and 3.8% (for **1**, **7** and **10**, respectively). Employing a similar analysis as for the photoxidation reaction gives 4.502 hr^{-1} for the rate constant, which again shows significant variability and non-monotonicity. Subsequently applying this value for the stated reaction time in continuous flow (24 minutes, 0.4 hours in the 25°C reactor) increases conversion of **3** to 83.5% (Seeberger et al., 2014).

Using reported data, the conversion of intermediate **4** (67.0%) was similarly calculated using the overall yield of byproduct **6** (6.1%, based on initial DHAA amount) (Kopetzki et al., 2013). Byproduct **6** is not of commercial interest here but must be taken into account in determining byproduct and impurity levels, key in final API separation operations and product quality and purity requirements.

Kopetzki et al. (2013) report small quantities of unspecified by-product from the photo-oxidation reaction. At less than 1% by moles, these have been assumed negligible, and the values for selectivity

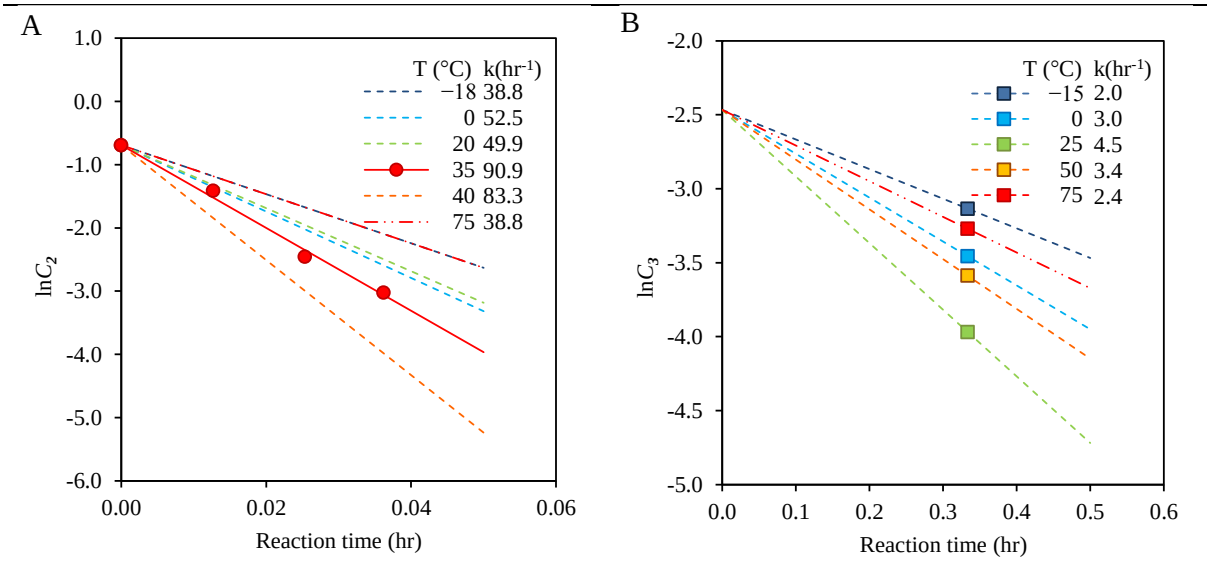

Fig. 4. Determination of rate constant used in this design. A: DHAA photooxidation (Table 3) (Seeberger et al., 2014). B: Reaction of intermediate **3** (Table 4) (Seeberger et al., 2014).

Table 3. Temperature-conversion-selectivity data for photo-oxidation of **2** (DHAA) into intermediates **3**, **4** and **5** (Seeberger et al., 2014).

Temperature (°C)	Conversion (%)	Selectivities (%)			
	X_2	S_3	S_4	S_5	S_{other}
−18	86	82	10	3	5
0	93	79	11	3	7
20	92	77	11	5	7
40	99	73	12	5	10
75	86	62	10	5	24

given here have been adjusted slightly to account for the difference. For the reactions occurring in the second PFR, the balance of yield based on initial DHAA is assumed to be unreacted species **3**. For PFR design, small internal diameters of 5 mm have been studied to ensure adequate heat transfer; proven CPM systems with designs at this length scale have been reported (Mascia et al., 2013).

The PFRs presented here have been designed using the standard plug flow reactor performance equation for a first-order reaction:

$$\tau_i = C_{A,0} \int_0^{X_{A,f}} \frac{dX_A}{-r_A} \tag{1}$$

The static model assumes homogeneous mixtures and ideal solutions with isothermal operation. The PFRs are assumed to be submerged in well circulating heat transfer media that ensures that there are no temperature gradients, with specific heat capacities and reaction enthalpies remaining constant; phase change also does not occur. There are also no radial concentration gradients, and mass transfer between the gaseous O_2 component and the liquid stream is assumed to not be reaction limiting. The small PFR dimensions considered ensure that the assumptions of excellent heat and mass transfer remain valid.

4 FINAL SEPARATION

The continuous synthesis route shown here will produce a range of organic intermediates and byproducts which must be removed in final purification separation. In the lab-scale demonstration of this continuous synthesis, multiple batch operations were used, consisting of extraction, evaporation, filtration, recrystallisation, and washing stages (Kopetzki et al., 2013; Seeberger et al., 2014). Suitable continuous separation alternatives must be found to fully capitalize on and demonstrate the benefits of CPM. Furthermore, for further processing the product API is required in pure solid form for downstream operations and final formulation (unless it will be used to produce artemisinin derivatives).

The reported efficiencies of the batch separation scheme used by Kopetzki et al. (2013) have been used to determine potential base-case process efficiencies such as product recovery and solvent use.

For this conceptual continuous flowsheet, continuous extraction operations were investigated for

Table 4. Temperature-yield (based on initial DHAA) data for reaction of **3** into byproducts and API **1** (a: estimated) (Seeberger et al., 2014).

Temperature (°C)	Conversion[a](%)	Yield (%)			
	X_2	$Y_{1(API)}$	Y_6	Y_7	Y_{10}
−15	49	18.0	1.6	2.1	21.3
0	63	33.4	3.7	2.1	17.8
25	78	59.1	6.1	4.4	2.5
50	67	47.0	7.2	5.5	4.7
75	55	31.2	7.5	6.1	9.6

trifluoroacetic acid (TFA) removal. Firstly, the use of counter-current extraction was investigated; however, the low initial amounts of TFA (approximately 2.5 mole %) and tie-line behaviour of the calculated TFA-toluene-water ternary phase diagram implies that this is impractical. Instead, the potential of a continuous two-phase agitated tank with subsequent phase settling and separation was investigated. In this idealised design, the dispersed organic phase (toluene) is injected into the continuous phase (water-$NaHCO_3$ solution) with agitation from an impeller. As acid-base reactions are almost instantaneous, with rate constants over the order of 10^8 s^{-1} reported (Pines et al., 1997), given sufficient bulk mixing the reaction should then be limited by the rate of mass transfer of TFA from the dispersed organic (toluene) droplets to the continuous water phase, which can be represented using the following equation:

$$\dot{N}_{TFA} = K_W A'\left(C^*_{TFA,W} - C_{TFA,W}\right) \tag{2}$$

Where $\dot{N}_{TFA}$ is the molar transfer rate of TFA, A' is the interfacial area (between dispersed organic drops and bulk aqueous phase), $C_{TFA,W}$ is the concentration of TFA in the aqueous phase, and $C^*_{TFA,W}$ is $C_{TFA,W}$ at equilibrium. The overall mass transfer coefficient K_W is calculated from the organic- and water-side film transfer coefficients k_O (from dispersed phase Sherwood number Sh_d) and k_w (from the continuous phase Sherwood number, using the Skelland-Moeti correlation) (Skelland and Moeti, 1990):

$$\frac{1}{K_W} = \frac{1}{mk_O} + \frac{1}{k_W} \tag{3}$$

$$Sh_d = \frac{k_O d_{32}}{D_{TFA,O}} = 6.6 \tag{4}$$

$$Sh_W = \frac{k_W d_{32}}{D_{TFA,W}} = 1.27\times10^{-5} Sc_W^{1/3} Fr_W^{5/12} Eo^{5/4} \varphi^{-1/2} Re_i^{2/3} \left(\frac{D_i}{d_{32}}\right)^2 \left(\frac{d_{32}}{D_t}\right)^{1/2} \tag{5}$$

Here, $D_{TFA,O/W}$ is the diffusivity of TFA in toluene (O) or water (W), d_{32} is the Sauter mean droplet diameter (of the dispersed toluene droplets), Sc_W and Fr_W are respectively the Schmidt and Froude numbers of the continuous phase, Eo is the Eotvos number, φ is the dispersed phase volume fraction,

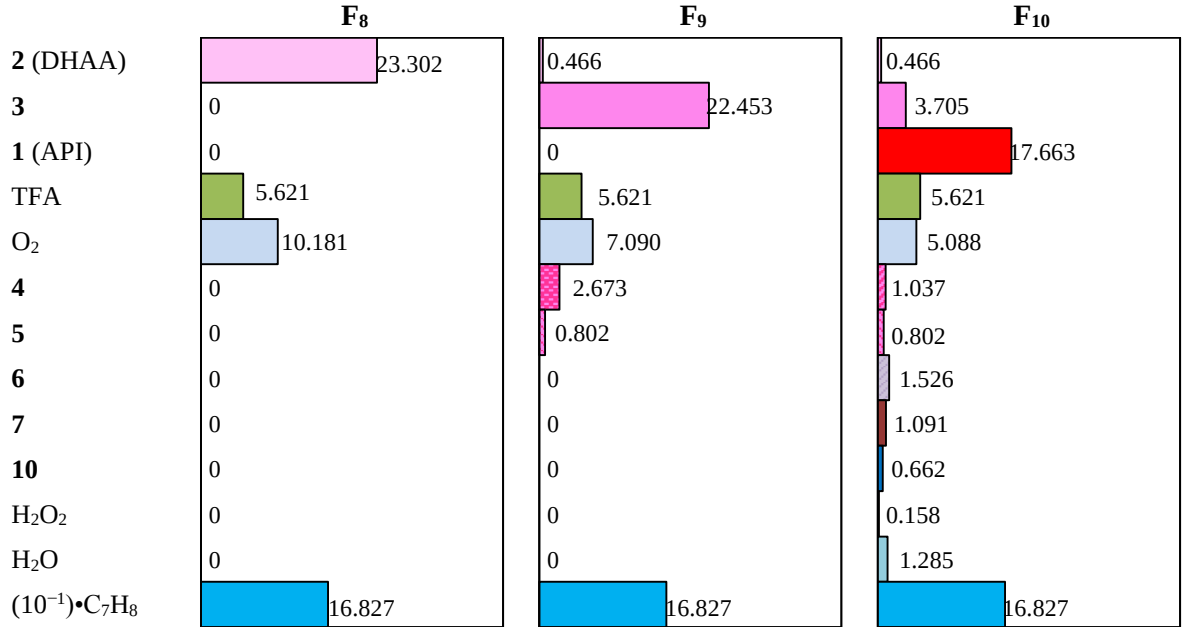

Fig. 5. Mass balance of key flowsheet streams (g hr^{-1}).

Re_i is the impeller Reynolds number, D_i and D_t are respectively the impeller and tank diameters. As TFA is miscible in both toluene and water, the partition coefficient m is unity. Equation (1) can then be used to estimate the potential for TFA extraction by varying parameters including φ and tank dimensions and operation.

In published examples, following batch acid extraction, toluene is removed by evaporation under reduced pressure, with the resultant solid dissolved in acetonitrile and then refluxed with activated carbon, which is then filtered off; this removes DCA. The solvent is then again evaporated off under reduced pressure; the solid proceeds to recrystallisation steps using cyclohexane and ethanol.

Although effective at recovering and purifying the API in the lab, alternatives to this procedure are required for industrial scale CPM use. In batch pharmaceutical production, solvent swaps are frequent due to their varying suitability in different applications; the best solvent for a reaction may not be suitable for a subsequent operation. However, solvent swaps are costly in terms of energy and material waste, and also take time. Another benefit of continuous production is that, almost exclusively, a single primary solvent is used (except where separations are required, e.g. liquid-liquid extraction, or anti-solvents for crystallisation). Here, we investigated the potential for toluene to be kept as a solvent, and an anti-solvent introduced, to replace the batch recrystallisation procedures using cyclohexane and ethanol. The UNIFAC method for estimating activity coefficients was used toward calculating artemisinin solubilities (see Appendix) (Gracin et al., 2002).

5 RESULTS AND DISCUSSION

5.1 Mass balance and reactor design

The continuous design presented here produces artemisinin at a rate of 17.66 g hr^{-1}, corresponding to 141.28 kg annual production (prior to separation) for 8,000 annual operating hours. A summary of key flowsheet stream mass balances is illustrated in Fig. 5. The mass balances are based on published kinetics and conversions for the reactions (Kopetzki et al., 2013; Seeberger et al., 2014).

The experimental demonstration achieved recoveries of 87.7% and 80.7% in the recrystallisation stages, for an overall product recovery of 70.8% (although it is reported that marginally higher recoveries are attainable) (Seeberger et al., 2014). Assuming that similar performance can be achieved by scaling up the batch scheme to mass flows used here, this recovers 12.5 g hr^{-1}, or 100.0 kg per year of API. The mass flow to this point has been used as a preliminary level to produce this benchmark annual quantity of API, allowing subsequent evaluation of continuous separation operations with regards to mass flows required.

Toluene (C_7H_8) is the organic solvent. The key species are feedstock **2** (DHAA), intermediate **3**, and **1** (artemisinin, the API product). In addition to these key organic molecules, various byproducts are present: species **4** and **5** are produced alongside **3** (although at far lower selectivity), while **7** and **10** also originate from **3**. TFA acts as acid catalyst here, and so is never consumed. DCA, the photosensitizer, is present in quantities too low to display in Fig. 5.

Small sizes have been calculated for the two reactors, with 19.722 mL for PFR1 and 78.923 mL for PFR2 (Table 5). Small internal diameters of 5.0 mm were studied to ensure that there is excellent heat and mass transfer. CPM pilot plant systems have been successfully demonstrated at this scale, with heat transfer ID = 1.6 mm and reactor ID = 11.7 to 40 mm, respectively (Mascia et al., 2013). Process simulations have also been performed at the reported capacity and compared to the published reactor dimensions implemented in the laboratory-scale experimental system (Kopetzki et al., 2013). These reactor sizes are for the production capacity presented in Fig. 5: larger capacities will require larger reactors, assuming one system is used.

Table 5. PFR design results.

PFR # (reaction)	Temperature (°C)	Flowrate (g hr^{-1})	Conversion (%)	*ID* (mm)	Volume (mL)	Length (mm)
PFR 1 (**2** → **3**)	−20	207.48	98.0	5.0	19.722	1005
PFR 2 (**3** → API)	25	207.48	83.5	5.0	78.923	4020
(**4** → **6**)	25	207.48	67.0	5.0	78.923	4020

Kopetzki et al. (2013) report an overall yield of 65% for artemisinin, which is close to the value calculated here (63.5%). More detailed experimental investigations for the full continuous process will elucidate the contributing factors to this small variation: as stated previously, in the full experimental demonstration toluene is used as a solvent with DCA as photosensitizer, while the value of 63.5% was computed on the basis of the marginally lower performance of DCM and TPP (solvent and photosensitizer, respectively). Moreover, the extent to which reactions may occur in the process lines between reactors is not taken into consideration here. While this is expected to be minimal, Kopetzki et al. (2013) do have an additional small pre-heating line at 10°C between the two reactors.

In the demonstration of the continuous chemical synthesis the reaction line was coiled around a transparent plate and placed near a mercury lamp (Kopetzki et al., 2013). The optimal configuration for maximum energy efficiency could be different, and multiple options are possible, including wrapping the reaction line in a coil with the lamp down the centre (Peplow, 2012). Here, the lamp along with exact configuration of the reactor are assumed to provide the necessary light for the photooxidation reaction.

5.2 Final separation

The product stream F_{10} requires separation and purification of the API product, artemisinin (**1**). The batch scheme utilised in the demonstration of the continuous chemical synthesis is illustrated in Fig. 6, where flows SF_1 - SF_{18} are not true streams but illustrate the use and movement of material to and from stages; SF_1 corresponds to the effluent stream of PFR2, which is CPM flowsheet stream F_{10}. An extraction with aqueous sodium bicarbonate first removes trifluoroacetic acid (TFA); this is followed by washing with brine and water. The organic phase then proceeds to a solvent removal stage where toluene is removed: this consists of drying with sodium sulfate, concentration using reduced pressure, followed by acetonitrile addition and subsequent evaporation and then vacuum drying. The resulting solid is then dissolved in acetonitrile with added activated carbon (which captures poorly soluble DCA) and filtered, which removes the carbon (along with DCA). The filtration product is then recrystallised using cyclohexane and ethanol in multiple steps, resulting in the API product in solid form (Kopetzki et al., 2013; Seeberger et al., 2014). These operations are suitable for lab scale

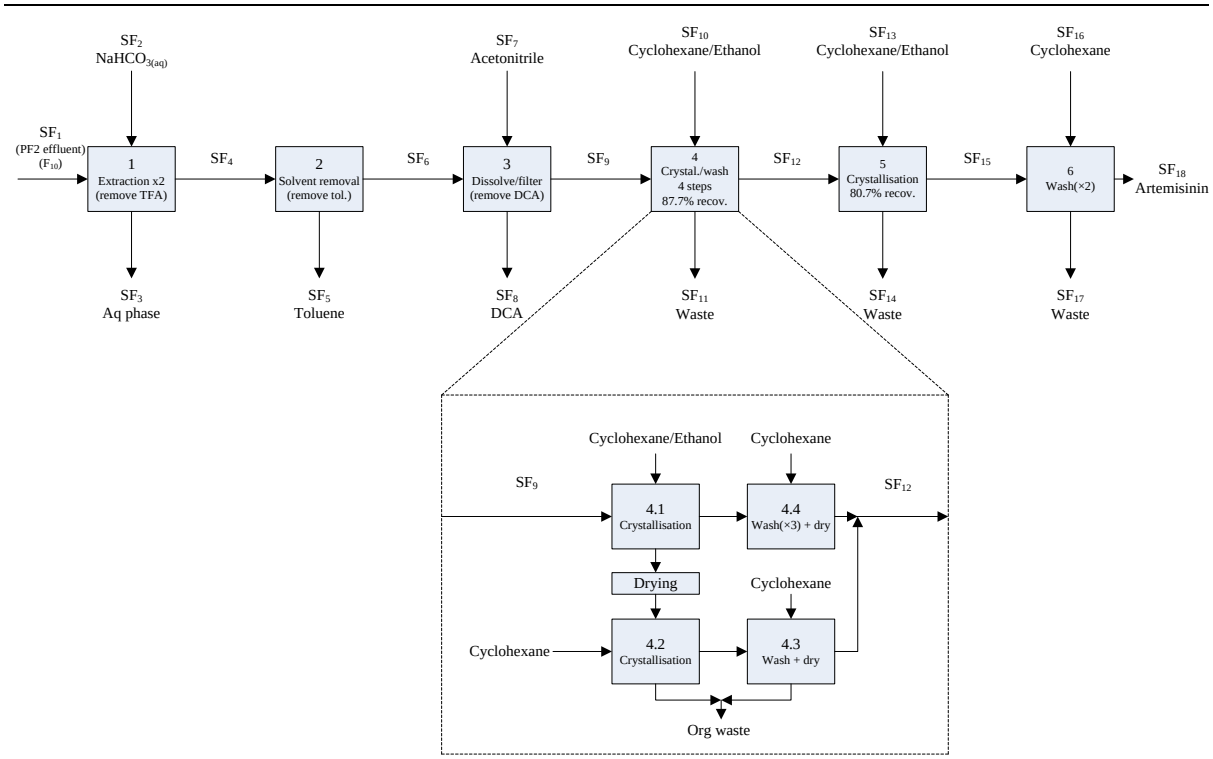

Fig. 6. Batch separation scheme for artemisinin purification according to the original flow synthesis method considered (Kopetzki et al., 2013).

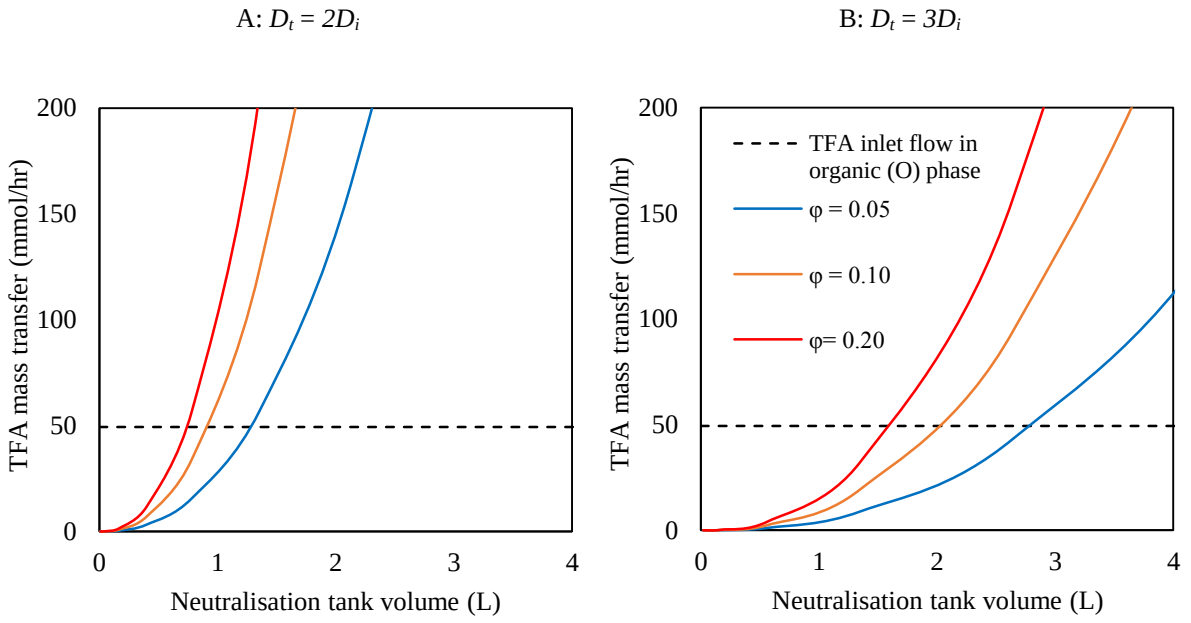

Fig. 7. Variation of potential mass transfer of TFA with tank volume and dispersed phase (organic) volume fraction (φ). A: Tank diameter (D_t) 2 times the impeller diameter (D_i). B: Tank diameter (D_t) 3 times the impeller diameter (D_i).

purification (where such steps are known as workup), but implementation of the continuous scheme in production scale requires continuous alternatives.

For the continuous extraction of TFA form the organic phase, the use of an agitated tank was investigated, where the organic phase (toluene) is dispersed into the aqueous phase. Sodium bicarbonate, saturated in the aqueous phase, neutralises the TFA. Oxygen and any other gaseous components are assumed removed prior to this by simple venting, with the process now at atmospheric pressure. Adjustable parameters affecting the estimation of TFA molar mass transfer from the toluene to the water include the impeller speed (set a high but attainable 15 rev/s), impeller diameter, tank diameter (two or three times the impeller diameter) and dispersed phase volume fraction (set with an upper limit of 0.2).

The inlet flow of TFA at this point in the flowsheet (entering an agitated tank) is 49.3 mmol hr^{-1} (Fig. 7, black dashed line). As illustrated by Fig. 7, mass transfer of TFA is favoured by higher dispersed phase volume fractions and impeller sizes (illustrated here by tank volumes, which are tied to impeller dimensions). Naturally, there are practical limits to both of these, particularly the volume fractions. Furthermore, higher ratios of impeller diameter to tank diameter (Fig. 7B) result in higher required volumes for a given mass transfer rate; however, smaller impellers do tend towards higher

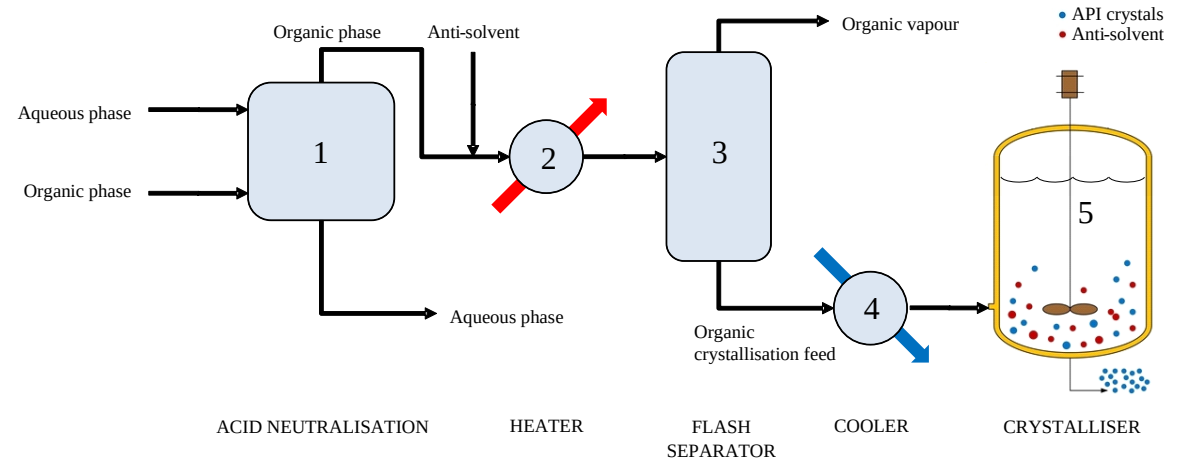

Fig. 8. Generalised schematic for continuous separation.

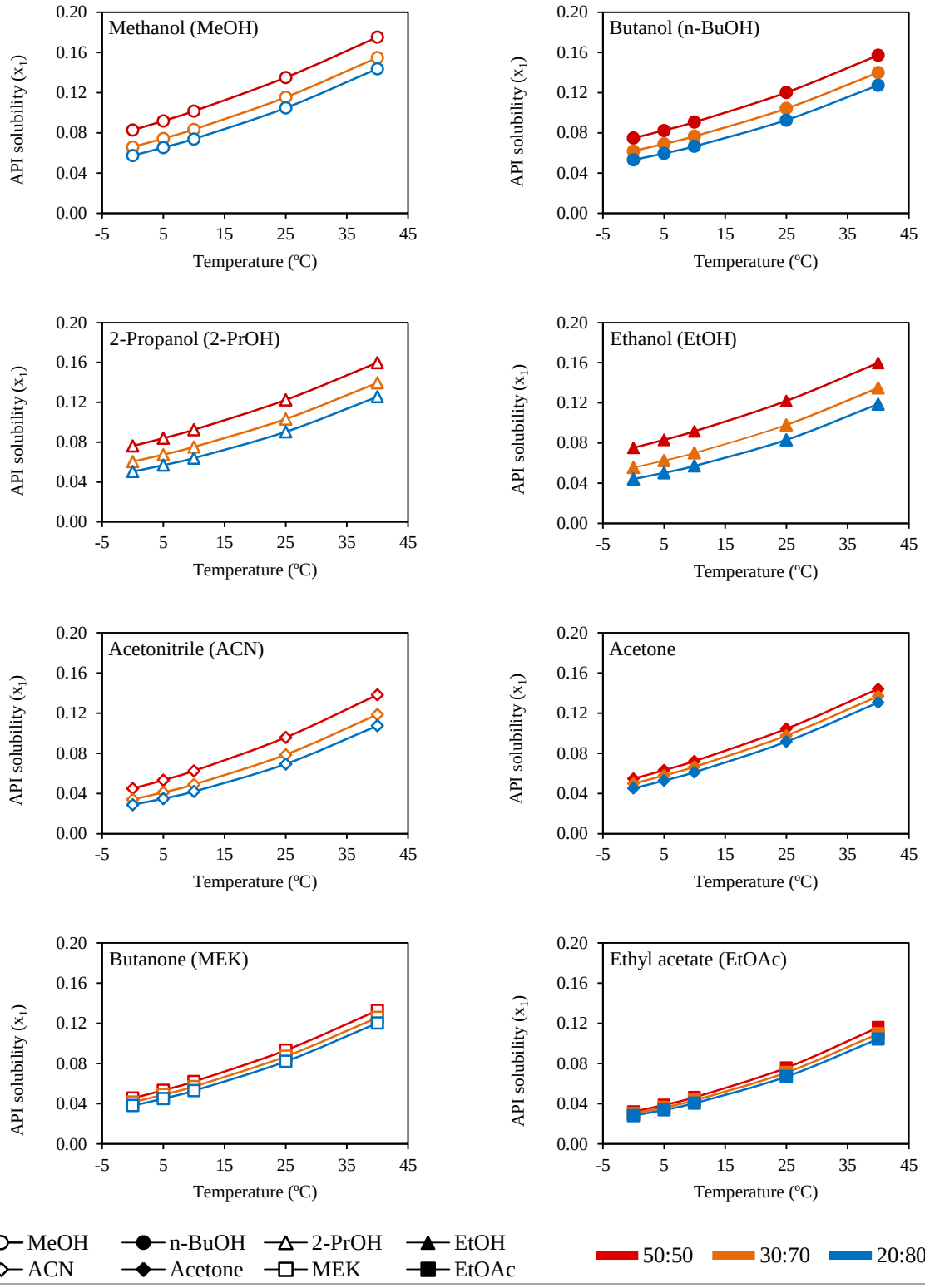

Fig. 9. Artemisinin solubility evaluation of potential anti-solvents for continuous crystallisation using the UNIFAC activity coefficient prediction method. Solvents appear in order of decreasing API solubility. The vertical axis is in units of mole fraction.

energy efficiency.

Eight common solvents, many classed as desirable (with the lowest toxicity and environmental impact) by a solvent selection guide, were initially investigated as for potential antisolvents for use in a continuous crystallisation operation: ethanol (EtOH), acetone, ethyl acetate (EtOAc), methanol

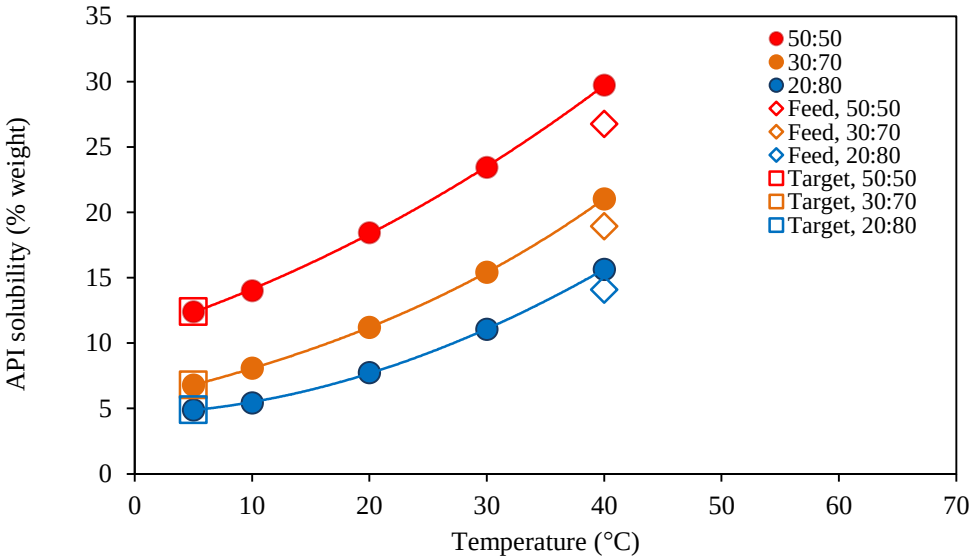

Fig. 10. Conceptual crystallisation operating parameters; empirical solubility data has been used (Horváth et al., 2015). System assumed to be composed of solute (API), solvent (toluene), and anti-solvent (EtOH) only.

(MeOH), 2-propanol (2-PrOH), n-butanol (n-BuOH), butanone (methyl ethyl ketone, MEK) and acetonitrile (ACN). All three are miscible with toluene, yet have a lower solubility of API. Artemisinin solubilities were evaluated for a temperature range of 0 to 40°C, for toluene-to-anti-solvent ratios of 50:50, 30:70, and 20:80 by weight (Fig. 9). An illustrative, generalised scheme of the design described here is given in Fig. 8.

Solubility increases with temperature in each case, while some candidate anti-solvents (Acetone, EtOAc, MEK) show little solubility variation between different solvent-to-anti-solvent ratios. Additional ratios, with toluene in the majority, were also studied, however in these cases anti-solvent addition increased predicted artemisinin solubilities, likely due to toluene being non-polar (results not shown). The use of ethyl acetate (EtOAc) is predicted to produce the lowest artemisinin solubilities. Recently published experimental solubility data for the toluene-ethanol system implies that the values computed through UNIFAC here are an over-prediction (Horváth et al., 2015). The complex molecular structure of artemisinin, along with the unavailability of some group interaction parameters,

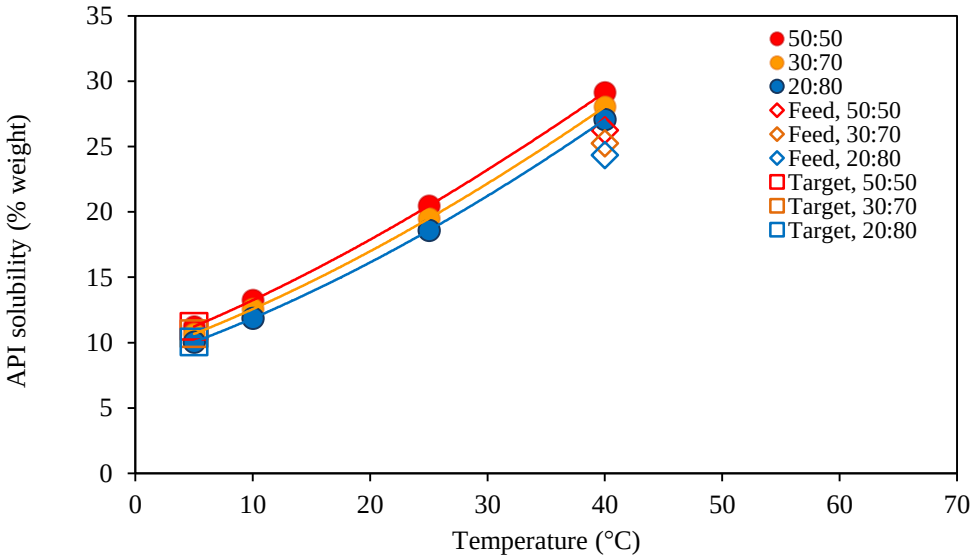

Fig. 11. Conceptual crystallisation operating parameters; calculated using the UNIFAC method – see Fig 8. EtOAc. System assumed to be composed of solute (API), solvent (toluene), and anti-solvent (EtOAc) only.

Table 6. Comparison of batch vs. continuous API recovery: EtOH anti-solvent.

		Batch	CPM		
			1	2	3
Production capacity (kg year^{-1})		**100**	**100**	**100**	**100**
PFR outflow (g hr^{-1})	**2** (DHAA)	0.47	0.61	0.51	0.51
	3	17.66	23.30	19.49	19.17
	1 (API)	5.62	7.41	6.20	6.10
	TFA	5.09	6.71	5.61	5.52
	O_2	3.70	4.89	4.09	4.02
	4	1.04	1.37	1.14	1.13
	5	0.80	1.06	0.88	0.87
	6	1.53	2.01	1.68	1.66
	7	1.09	1.44	1.20	1.18
	10	0.66	0.87	0.73	0.72
	H_2O_2	0.16	0.21	0.17	0.17
	H_2O	1.28	1.69	1.42	1.39
Solvent (g hr^{-1})	Toluene	168.27	221.95	185.65	182.61
Solvent : antisolvent (weight : weight)		**-**	**50:50**	**30:70**	**20:80**
Separation (g hr^{-1})	ACN	19.80	-	-	-
	Cyclohexane	587.80	-	-	-
Antisolvent (g hr^{-1})	EtOH	18.60	56.65	107.02	189.53
	EtOAc	-	-	-	-
Thermodynamic API recovery (%)		70.1	53.7	64.1	65.2
Waste (g hr^{-1})	API	5.16	10.80	6.99	6.67
	Unrecovered solvents	794.51	253.84	244.11	276.17
	Others (excl. O_2)	16.35	21.57	18.04	17.75
	Total	816.03	286.21	269.14	300.58
E-factor		65.28	22.90	21.53	24.05

are plausible explanations for this discrepancy. For further design, the experimental solubility data from Horváth et al. (2015) were used, employing ethanol as antisolvent with suitable feed API concentrations studied for each case of antisolvent amount (90% of saturation, or 26.8%, 18.9%, and 14.1% by mass for 50:50, 30:70 and 20:80 of toluene : EtOH, respectively) (Fig. 10). This was compared with the use of ethyl acetate (EtOAc) as anti-solvent, studying similar feed API concentrations of (90% saturation, or 26.2%, 25.2% and 24.4% by mass (for 50:50, 30:70 and 20:80 of toluene : EtOAc, respectively) using solubility data calculated via the UNIFAC method (Fig. 11).

Stream concentration to lower solvent amount is required for efficient crystallisation: antisolvent addition without API concentration results in low feed API mass percentages with which crystallisation cannot be performed (i.e. concentration is below the solubility that would be reached at the bottom of the temperature range). In order to achieve the desired feed API concentrations, anti-solvent must first be added, as toluene evaporation alone will exceed API saturation (Liu et al., 2009). The required anti-solvent quantities to be added prior to evaporation in each case were calculated by performing isothermal flash calculations in the UniSim® software package (Honeywell, 2014). The predicted solubilities achieved from the use of ethyl acetate (Fig. 11) are higher than experimental solubilities for ethanol use (Fig. 10), however there is less variation with quantity of antisolvent.

Table 7. Comparison of batch vs. continuous API recovery: EtOAc anti-solvent.

		Batch	CPM		
			4	**5**	**6**
Production capacity (kg year^{-1})		**100**	**100**	**100**	**100**
PFR outflow (g hr^{-1})	**2** (DHAA)	0.47	0.58	0.57	0.56
	3	17.66	21.86	21.65	21.27
	1 (API)	5.62	6.95	6.89	6.77
	TFA	5.09	6.30	6.24	6.13
	O_2	3.70	4.58	4.54	4.46
	4	1.04	1.28	1.27	1.25
	5	0.80	0.99	0.98	0.97
	6	1.53	1.89	1.87	1.84
	7	1.09	1.35	1.34	1.31
	10	0.66	0.82	0.81	0.80
	H_2O_2	0.16	0.20	0.19	0.19
	H_2O	1.28	1.59	1.57	1.55
Solvent (g hr^{-1})	Toluene	168.27	208.21	206.25	202.65
Solvent : antisolvent (weight : weight)		**-**	**50:50**	**30:70**	**20:80**
Separation (g hr^{-1})	ACN	19.80	-	-	-
	Cyclohexane	587.80	-	-	-
Antisolvent (g hr^{-1})	EtOH	18.60			
	EtOAc		30.72	44.90	52.84
Thermodynamic API recovery (%)		70.1	57.2	57.7	58.8
Waste (g hr^{-1})	API	5.16	9.36	9.15	8.77
	Unrecovered solvents	794.51	238.92	251.15	255.49
	Others (excl. O_2)	16.35	20.24	20.04	19.69
	Total	816.03	268.51	280.34	283.96
E-factor		65.28	21.48	22.43	22.72

The API recovery that could be achieved was assumed to be the thermodynamically possible yield for each system, and on this basis the three continuous separation schemes (varying antisolvent use, for a temperature drop from 40°C in the feed to 5°C) for anti-solvent (ethanol and ethyl acetate) were compared with the experimentally employed batch scheme (Table 6 and Table 7, respectively). Annual operation was again assumed to be 8,000 hours.

Maximum product recoveries improve with increasing antisolvent use in the case of ethanol (between 53.7% to 65.2%), in contrast to ethyl acetate, for which they remain relatively constant (between 57.2% to 58.8%) (Figure 12); this is predominantly due to the solubility behaviour of the API in the antisolvent-solvent mixture. While ethanol is preferable based on product recoveries, taking into account additional metrics, particularly those related to environmental impact and safety, can significantly affect antisolvent preferability (Jolliffe and Gerogiorgis, 2016).

Varying product recoveries with rate of antisolvent use offer potential for process control. API productivity could be increased or maintained by adjusting the rate of antisolvent use if there were bottlenecks elsewhere in the process in terms of absolute mass throughput.

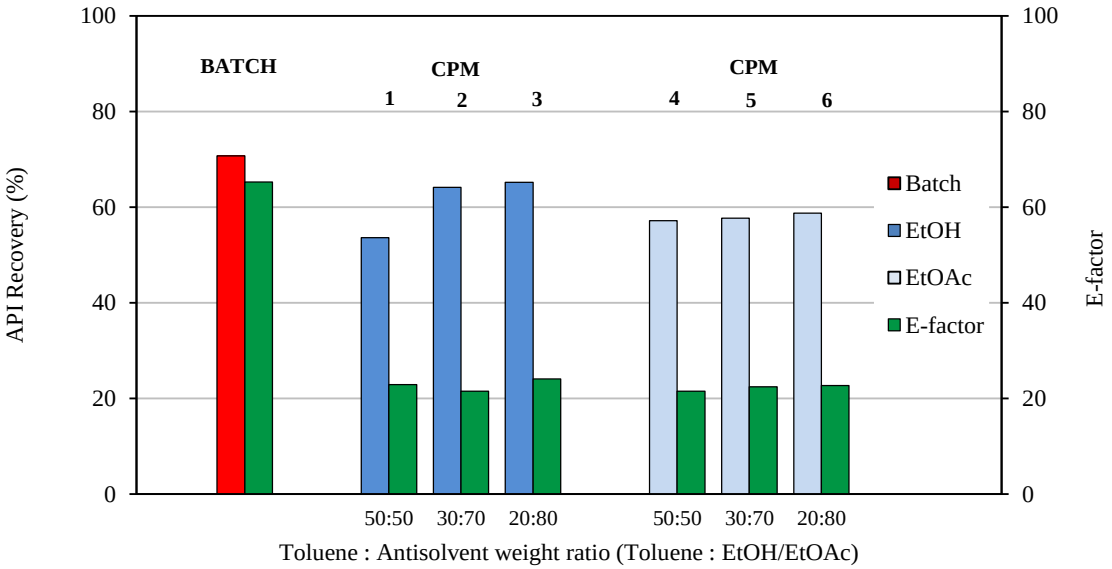

Fig. 12. Evaluation of batch and continuous separation schemes: API recovery and E-factor.

5.3 Environmental impact (E-factor)

A useful metric for quantifying environmental impact is the E-factor (Sheldon, 2012). It is versatile with multiple definitions, the simplest of which is the quantity of waste generated per unit of product, in mass terms. Sustainability metrics (Balomenos et al., 2014) and systematic model-based sensitivity analyses (Angelopoulos et al., 2013, 2014) acquire ever-increasing importance in the entire spectrum of chemical process industries, in order to assess profitability in tandem with environmental and societal responsibility. Highly efficient industries relying almost completely on continuous production techniques – such as oil and gas – have E-factors in the order of 0.1, while batch-reliant processes such as pharmaceutical production generate significant relative amounts of waste with high E-factors of 200 not uncommon (Ritter, 2013). Here, the E-factor is computed where the product is (pure) recovered API, while the waste consists of byproducts (bpd), unconverted reactants (ur), waste solvent (ws, all assumed unrecovered), and unrecovered API (uAPI):

$$E = \frac{m_{waste}}{m_{API}} = \frac{m_{bpd} + m_{ur} + m_{ws} + m_{uAPI}}{m_{API}} \tag{6}$$

Material requirements for TFA removal have not been included in E-factor calculations as water is the main component in this stage, and due to its negligible environmental impact cost is commonly excluded (Sheldon, 2012). Moreover, this operation is upstream of the subsequent API separation and general E-factor trends would remain unaffected. The solvents have been assumed to be unrecovered, while unused O_2 has been assumed to have been recovered via simple phase separation after exiting the last reactor.

For the batch scheme outlined in Fig. 6, the calculated E-factor is 65.28: for every kilogram of API pure API obtained, 65.28 kilograms of waste are generated. This is very likely an underestimation, as specific quantities of chemical used were not available for all of the operations detailed in Fig. 6 (Seeberger et al., 2014). Solvents form the bulk of the waste (794.5 g/hr).

Based on the assumed feed concentrations (post-solvent evaporation), calculated E-factor values are better (lower) for the six studied CPM scenarios in comparison to the batch case, ranging from 21.48 to 24.05 (Table 6, Table 7, Fig. 12). This implies that for a unit of API produced, the CPM schemes generate on average 66.2% less waste than the batch process. While high compared to industries exclusively using continuous processes, these values are acceptably low given that typical pharmaceutical processes have significantly worse values. Although product recoveries are lower for the CPM cases than the batch case (CPM: 53.7-64.1%, batch: 70.1%), this is offset by the significant reduction in waste. Moreover, it must be noted that the separation scheme employed would not be implemented industrially: while high recoveries are achieved, the required timescale of the batch

operations was not a consideration, with maximum product recovery the goal. In addition, although material requirements are likely to change and E-factors worsen with more detailed design of CPM separation cases, they nevertheless show promise, and it is unlikely that only a single crystallisation stage would be employed. Additional stages or other separation technologies can be used to greatly enhance performance (Horváth et al., 2015).

The differences between E-factors calculated for the use of ethanol (Table 6) or ethyl acetate (Table 7) are small, ranging from 21.43-24.05 and 21.48-22.72, respectively, an average difference of only 2.7%. The use of ethanol results in higher API recoveries, with the exception of 50:50 toluene : ethanol use. Product recoveries increase with anti-solvent use: for both antisolvents, recovery is lowest for 50:50 toluene : antisolvent and highest for 20:80. Due to the smaller influence of antisolvent quantity on API solubility (Fig. 10), there is less variation in recovery when ethyl acetate is used.

Given the similar performances of the two antisolvents studied here, additional factors such as compatibility with subsequent (or additional prior) separation operations require investigation for accurate evaluation. Nevertheless, on the basis of the calculations and analysis presented here, the use of ethanol in a 20:80 ratio with toluene by weight (CPM case 3, Fig. 12) is to be favoured: it results in the highest API recoveries, while the E-factor (i.e. waste generated) is only marginally more than the other CPM cases, but significantly less than the batch case.

6 CONCLUSIONS

The Continuous Pharmaceutical Manufacturing (CPM) of the key antimalarial substance artemisinin has been presented in this paper. Multiple designs with different continuous product recoveries have been compared with a batch reference case, with all designs producing 100 kg of API per year. The chemistry this study is based on is of particular interest due to the feedstock being a waste product of current artemisinin production: significant added value is possible from implementing this design alongside established artemisinin production plants.

Employing published reaction data novel kinetic data analysis and parameter estimation have been performed, allowing the computation of small reactor volumes (19.72 mL and 78.72 mL) have been computed based on published reaction data, implying capital cost and space advantages which are hallmark benefits of continuous production.

An environmental (E-) factor of 65.28 has been estimated for a reference case design studying reported performances of a batch separation scheme, an acceptable value for a process employing some batch operations. Evaluations of potential continuous alternatives, using published solubility data as well as the UNIFAC method, indicate good performance with improved E-factors ranging from 21.48 to 24.05, with ethanol and ethyl acetate good anti-solvent candidates in a crystallisation process; the small decrease in product recovery for continuous separation (70.1% for batch, up to 65.2% for continuous designs) is offset by significantly reduced waste production compared to the batch process. Investigation of a continuous alternative for acid neutralisation illustrates the scope for using continuous agitated tanks.

Artemisinin is a substance of critical importance. An effective anti-malarial itself, it is the precursor to many anti-malarial derivatives which are widely used to combat a disease of significant impact. The use of a current waste material for feedstock gives significant added value to the implementation of this design, which is an excellent opportunity for demonstrating CPM benefits. The potential use of a widely used solvent of low toxicity and environmental impact in a continuous alternative separation illustrates how green processing ideals can be met with systematic design. To further demonstrate the potential of this design, a full investigation of an integrated continuous separation process is required; this is of particular importance for downstream processing.

The need and benefits of full process simulations of this design, which have been technically and economically optimised, emerges from this study. The use of a systematic framework and design methods will be of paramount importance in continuing to build the case for CPM.

ACKNOWLEDGEMENT

The authors gratefully acknowledge the financial support of the Engineering and Physical Sciences Research Council (EPSRC) via a Doctoral Training Partnership (DTP) studentship to Mr H.G. Joliffe.

NOMENCLATURE

Latin Letters

A'	Interfacial area, m^2
a^s	Pure solid component activity
C_A	Concentration of molecule *A*, mol L^{-1}
C^*_A	Equilibrium concentration of molecule *A*, mol L^{-1}
$C_{A,0}$	Initial concentration of molecule *A*, mol L^{-1}
$C_{A,W}$	Aqueous phase concentration of molecule *A*, mol L^{-1}
C_P	Specific heat capacity at constant pressure, J mol^{-1} K^{-1}
d_{32}	Sauter mean droplet diameter, m
$D_{A,O/W}$	Diffusivity of molecule A in organic/aqueous phase, m^2 hr^{-1}
D_i	Impeller diameter, m
D_t	Tank diameter, m
E	Environmental factor, dimensionless
Eo	Eotvos number, dimensionless
Fr_W	Aqueous (continuous) phase Froude number, dimensionless
ID	Internal diameter, mm
k'	Pseudo-first-order reaction rate constant, hr^{-1}
k_i	Rate constant of reaction *i*, L mol^{-1} hr^{-1} (second-order reaction)
k_O	Organic phase film mass transfer coefficient, m hr^{-1}
k_W	Aqueous phase film mass transfer coefficient, m hr^{-1}
K_W	Overall mass transfer coefficient, m hr^{-1}
L_i	UNIFAC compound parameter of *r*, *q* and *z*
m_{API}	Mass of recovered API
m_{bpd}	Mass of byproducts
m_{ur}	Mass of unconverted reactants
m_{ws}	Mass of waste solvent
m_{uAPI}	Mass of unrecovered API
MW	Molecular weight, g mol^{-1}
m_{waste}	Mass of waste
$\dot{N}_{TFA}$	Molar rate of trifluoroacetic acid transfer (mmol hr^{-1})
Q_k	UNIFAC surface area parameter for functional group *k*
q_i	UNIFAC parameter for molecule *i*, a measure of Van der Waals molecular surface area
R	Universal gas constant, 8.3144 J mol^{-1} K^{-1}
Re_i	Impeller Reynolds number, dimensionless
R_k	UNIFAC volume parameter for functional group *k*
r_A	Rate of reaction of molecule A, mol l^{-1} s^{-1}
r_i	UNIFAC parameter for molecule *i* , a measure of Van der Waals volume
S_i	Selectivity of species *i*
Sc_W	Aqueous (continuous) phase Schmidt number, dimensionless
Sh_d	Organic (dispersed) phase Sherwood number, dimensionless
Sh_W	Aqueous (continuous) phase Sherwood number, dimensionless
T	Temperature, K
T_{fus}	Melting (fusion) point temperature, K
t	Time, hr
U_{mn}	UNIFAC energy interaction between groups *m* and *n*
X_A	Conversion of molecule *A* at time *t*
$X_{A,f}$	Final conversion of molecule *A*
x_i	Mole fraction of molecule *i*

x_m UNIFAC mole fraction of group *m*
x_i^{sat} Mole fraction at saturation (solubility)
Y_i Yield of species *i*
z UNIFAC system coordination number (default value: 10)

Greek Letters
Γ_k UNIFAC residual group activity coefficient for group *k*
$\Gamma_k^{(i)}$ UNIFAC residual group activity coefficient in a reference solution of 100% *i* molecules
γ_i Activity coefficient of component *i*
γ_i^{c} UNIFAC combinatorial component of γ_i
γ_i^{r} UNIFAC residual component of γ_i
γ_i^{sat} Activity coefficient of component *i* at saturation
ΔH_{fus} Enthalpy of fusion, J mol^{-1}
θ_i UNIFAC molar-weighted area fractional component for molecule *i*
θ_m UNIFAC summation of area fraction of group *m* over all different groups
$v_k^{(i)}$ UNIFAC number of occurrences of functional group *k* in molecule *i*
φ Dispersed phase volume fraction
τ_i Residence time in reactor *i*, hr
ϕ_i UNIFAC molar-weighted segment fractional component molecule *i*
Ψ_{mn} UNIFAC group energy interaction parameter

LITERATURE REFERENCES

1. Abdin, M.Z., Alam, P., 2015. Genetic engineering of artemisinin biosynthesis: prospects to improve its production. *Acta Physiol. Plant.* **37**(2): 1–12.
2. Abrams, D.S., Prausnitz, J.M., 1975. Statistical thermodynamics of liquid mixtures: a new expression for the excess Gibbs energy of partly or completely miscible systems. *AICHE J.* **21**(1): 116–128.
3. Amara, Z., Bellamy, J.F.B., Horvath, R. et al., 2015. Applying green chemistry to the photochemical route to artemisinin. *Nat. Chem.* **7**(6): 489–495.
4. Anderson, N.G., 2012. Using continuous processes to increase production. *Org. Process Res. Dev.* **16**(5): 852–869.
5. Angelopoulos, P.M., Gerogiorgis, D.I., Paspaliaris, I., 2013. Model-based sensitivity analysis and experimental investigation of perlite grain expansion in a vertical electrical furnace. *Ind. Eng. Chem. Res.* **52**(50): 17953–17975.
6. Angelopoulos, P.M., Gerogiorgis, D.I., Paspaliaris, I., 2014. Mathematical modeling and process simulation of perlite grain expansion in a vertical electrical furnace. *Appl. Math. Model.* **38**(5): 1799–1822.
7. Balomenos, E., Giannopoulou, I., Gerogiorgis, D.I. et al., 2014. Resource-efficient and economically viable pyrometallurgical processing of industrial ferrous by-products. *Waste Biomass Valori.* **5**(3): 333–342.
8. Behr, A., Brehme, V. A., Ewers, C.L.J., Grön, H., Kimmel, T. et al., 2004. New developments in chemical engineering for the production of drug substances. *Eng. Life Sci.* **4**(1): 15–24.
9. Bionexx, 2014. Aligning artemisinin and ACT supplies. URL: http://www.rollbackmalaria.org/files/files/partnership/wg/wg_procurementsupply/docs/11_CGIBLAINMadagascarAfricaReport.pdf. [27/7/2015].
10. Bogdan, A.R., Poe, S.L., Kubis, D.C. et al., 2009. The continuous-flow synthesis of ibuprofen. *Angew. Chem. Int. Ed.* **48**(45): 8547–8550.
11. Corsello, M.A., Garg, N.K., 2015. Synthetic chemistry fuels interdisciplinary approaches to the production of artemisinin. *Nat. Prod. Rep.* **32**(3): 359–366.
12. Cutler, M., 2013. Artemisinin Conference 2013, Nairobi, Kenya, 14–16th January 2013.
13. Davis, W.A., Clarke, P.M., Siba, P.M. et al., 2011. Cost-effectiveness of artemisinin combination therapy for uncomplicated malaria in children: data from Papua New Guinea. *Bull. World Health Organ.* **89**(3): 211–220.
14. Ellmann, A., 2010. Cultivation of *Artemisia annua*: implications of intensification. Artemisinin Conference 2010, Madagascar, 12–14th October 2010.
15. Extance, A., 2012. Tube-wrapped lamp makes malaria drug. *Royal Society of Chemistry: Chemistry World*. URL: http://www.rsc.org/chemistryworld/News/2012/January/malaria-flow-reactors-artemisinin-Seeberger.asp. [27/7/2015].
16. Fredenslund, A., Jones, R.L., Prausnitz, J.M., 1975. Group-contribution estimation of activity coefficients in nonideal liquid mixtures. *AICHE J.* **21**(6): 1086–1099.

17. Gernaey, K.V., Cervera-Padrell, A.E., Woodley, J.M., 2012. Development of continuous pharmaceutical production processes supported by process systems engineering methods and tools. *Future Med. Chem.* **4**(11): 1371–1374.
18. Gerogiorgis, D.I., Barton, P.I., 2009. Steady-state optimization of a continuous pharmaceutical process. *Comp. Aid. Ch.* **27**(A): 927–932.
19. Gerogiorgis, D.I., Ydstie, B.E., 2003. A finite element computational fluid dynamics sensitivity analysis for the conceptual design of a carbothermic aluminium reactor. *Light Metals 2003*. The Minerals, Metals and Materials Society. 407–414.
20. Gerogiorgis, D.I., Ydstie, B.E., Bruno M. et al., 2003. Process systems tools for design and optimization of carbothermic reduction processes. *Aluminium 2003*: 407–414.
21. Gerogiorgis, D.I., Ydstie, B.E., 2005. Multiphysics CFD modelling for design and simulation of a multiphase chemical reactor. *Chem. Eng. Res. Des.* **83**(A6): 603–610.
22. Gilmore, K., Kopetzki, D., Lee, J.W. et al., 2014. Continuous synthesis of artemisinin-derived medicines. *Chem. Commun.* **50**(84): 12652–12655.
23. Gracin, S., Brinck, T., Rasmuson, Å.C., 2002. Prediction of solubility of solid organic compounds in solvents by UNIFAC. *Ind. Eng. Chem. Res.* **41**(20): 5114–5124.
24. Griffin, D.W., Mellichamp, D.A., Doherty, M.F., 2010. Reducing the mean size of API crystals by continuous manufacturing with product classification and recycle. *Chem. Eng. Sci.* **65**(21): 5770–5780.
25. Henry, R., 2014. Etymologia: Artemisinin. *Emerg. Infect. Dis.* **20**(7): 1217.
26. Hommel, M., 2008. The future of artemisinins: natural, synthetic or recombinant? *J. Biol.* **7**(10): 38.
27. Honeywell, 2014. Unisim® User Guide. URL: http://unisim.supportportal.com/ics/support/DLRedirect.asp?fileID=115045. [27/7/2015].
28. Horváth, Z., Horosanskaia, E., Lee, J.W. et al., 2015. Recovery of artemisinin from a complex reaction mixture using continuous chromatography and crystallization. *Org. Process Res. Dev.* **19**(6): 624–634.
29. Içten, D., Nagy, Z.K., Reklaitis, G.V., 2015. Process control of a dropwise additive manufacturing system for pharmaceuticals using polynomial chaos expansion based surrogate model. *Comput. Chem. Eng.* **83**: 221–231
30. Jolliffe, H.G., Gerogiorgis, D.I., 2015a. Process modelling and simulation for continuous pharmaceutical manufacturing of ibuprofen. *Chem. Eng. Res. Des.* **97**: 175–191.
31. Jolliffe, H.G., Gerogiorgis, D.I., 2015b. Plantwide design and economic evaluation of two continuous pharmaceutical manufacturing (CPM) cases: ibuprofen and artemisinin. *Comput. Chem. Eng.* In press.
32. Jolliffe, H.G., Gerogiorgis, D.I., 2016. Systematic solvent evaluation for artemisinin recovery in continuous pharmaceutical manufacturing. Presented at the ESCAPE26 International Conference on Computer-Aided Process Engineering - accepted, Elsevier, Portorož, Slovenia.
33. Kopetzki, D., Lévesque, F., Seeberger, P.H., 2013. A continuous-flow process for the synthesis of artemisinin. *Chem.-Eur. J.* **19**(17): 5450–5456.
34. Kwon, J.S.I., Nayhouse, M., Christofides, P.D., Orkoulas, G., 2013. Modeling and control of shape distribution of protein crystal aggregates. *Chem. Eng. Sci.* **104**: 484–497.
35. Kwon, J.S.I., Nayhouse, M., Orkoulas, G., Christofides, P.D., 2014a. Modeling and control of crystal shape in continuous protein crystallization. *Chem. Eng. Sci.* **107**: 47–57.
36. Kwon, J.S.I., Nayhouse, M., Orkoulas, G., Christofides, P.D., 2014b. Crystal shape and size control using a plug flow crystallization configuration. *Chem. Eng. Sci.* **119**: 30–39.
37. Lakerveld, R., Benyahia, B., Heider, P.L., Zhang, H., Wolfe, A. et al., 2015. The application of an automated control strategy for an integrated continuous pharmaceutical pilot plant. *Org. Process Res. Dev.* **19**(9): 1088–1100.
38. Lee, S.L., O'Connor, T.F., Yang, X. et al., 2015. Modernizing pharmaceutical manufacturing: from batch to continuous production. *J. Pharm. Innov.* Online First article (not assigned issue).
39. Lévesque, F., Seeberger, P.H., 2012. Continuous-flow synthesis of the anti-malaria drug artemisinin. *Angew. Chem. Int. Ed.* **51**(7): 1706–1709.
40. Li, A., Tang, S., Tan, P. et al., 2007. Measurement and prediction of oxygen solubility in toluene at temperatures from 298.45 K to 393.15 K and pressures up to 1.0 MPa. *J. Chem. Eng. Data* **52**(6): 2339–2344.
41. Liu, Y., Iue, H., Pang, F., 2009. Solubility of artemisinin in seven different pure solvents from (283.15 to 323.15) K. *J. Chem. Eng. Data* **54**(3): 762–764.
42. Mascia, S., Heider, P.L., Zhang, H., Lakerveld, R., Benyahia, B. et al., 2013. End-to-end continuous manufacturing of pharmaceuticals: integrated synthesis, purification, and final dosage formation. *Angew. Chem. Int. Ed.* **52**(47):12359–12363.
43. Miller, L.H., Su, X., 2011. Artemisinin: discovery from the Chinese herbal garden. *Cell* **146**(6): 855–858.
44. Nayhouse, M., Tran. A., Kwon, J.S.-I., Crose, M., Orkoulas, G., Christofides, P.D., Modeling and control of ibuprofen crystal growth and size distribution, *Chem. Eng. Sci.* **134**: 414–422.

45. Paddon, C.J., Keasling, J.D., 2014. Semi-synthetic artemisinin: a model for the use of synthetic biology in pharmaceutical development. *Nat. Rev. Microbiol.* **12**(5): 355–367.
46. Paddon, C.J., Westfall, P.J., Pitera, D.J. et al., 2013. High-level semi-synthetic production of the potent antimalarial artemisinin. *Nature* **496**(7446): 528–532.
47. Peplow, M., 2013. Sanofi launches malaria drug production. *Royal Society of Chemistry: Chemistry World*. URL: http://www.rsc.org/chemistryworld/2013/04/sanofi-launches-malaria-drug-production. [27/7/2015].
48. Pines, E., Magnes, B.-Z., Lang, M.J. et al., 1997. Direct measurement of intrinsic proton transfer rates in diffusion-controlled reactions. *Chem. Phys. Lett.* **281**(4-6): 413–420.
49. Plumb, K., 2005. Continuous processing in the pharmaceutical industry – changing the mind set. *Chem. Eng. Res. Des*. **83**(A6): 730–738.
50. Ritter, S.K., 2013. Reducing environmental impact of organic synthesis. *Chem. Eng. News.* **91**(15): 22–23.
51. Roberge, D.M., Zimmermann, B., Rainone, F. et al., 2008. Microreactor technology and continuous processes in the fine chemical and pharmaceutical industry: is the revolution underway? *Org. Process Res. Dev.* **12**(5): 905–910.
52. Schaber, S.D., Gerogiorgis, D.I., Ramachandran, R. et al., 2011. Economic analysis of integrated continuous and batch pharmaceutical manufacturing: a case study. *Ind. Eng. Chem. Res.* **50**(17): 10083–10092.
53. Seeberger, P.H., Kopetzki, D., Levesque, F., 2014. Method and device for the synthesis of artemisinin. US Patent Application US20140364630 A1.
54. Sheldon, R.A., 2012. Fundamentals of green chemistry: efficiency in reaction design. *Chem. Soc. Rev.* **41**(4): 1437−1451.
55. Skelland, A.H.P., Moeti, L.T., 1990. Mechanism of continuous-phase mass transfer in agitated liquid-liquid systems. *Ind. Eng. Chem. Res.* **29**(11): 2258–2267.
56. Teoh, S.K., Rathi, C., Sharratt, P., 2015. Practical assessment methodology for converting fine chemicals processes from batch to continuous. *Org. Process Res. Dev.* In press.
57. The Boston Consulting Group (BCG), 2009. Artemisinin scenario analysis. URL: https://www.york.ac.uk/org/cnap/artemisiaproject/work%20docs/Artemisinin%20Scenario%20Analysis.pdf. [27/7/2015].
58. The Nobel Assembly, 2015. The Nobel Prize in Physiology or Medicine 2015, press release. URL: http://www.nobelprize.org/nobel_prizes/medicine/laureates/2015/press.html. [10/10/2015].
59. Tu, Y.Y., Ni, M.Y., Zhong, Y.R. et al., 1981. [Studies on the constituents of Artemisia annua L. (author's transl)]. [Article in Chinese]. *Acta Pharm. Sinica* **16**(5): 366–370.
60. Tu, Y.Y., Ni, M.Y., Zhong, Y.R. et al., 1982. Studies on the constituents of Artemisia annua Part II. *Planta Med.* **44**(3): 143–145.
61. Tu, Y.Y., 2011. The discovery of artemisinin (qinghaosu) and gifts from Chinese medicine. *Nat. Med.* **17**(10): 1217–1220.
62. Turconi, J., Griolet, F., Guevel, R. et al., 2014. Semisynthetic artemisinin, the chemical path to industrial production. *Org. Process Res. Dev.* **18**(3): 417–422.
63. Wang, Z., Yang, L., Yang, X. et al., 2014. Advances in the chemical synthesis of artemisinin. *Synth. Commun.* **44**(14): 1987–2003.
64. Ward, J.D., Cheng-Ching, Y., Doherty, M.F., 2011. A new framework and a simpler method for the development of batch crystallization recipes. *AICHE J.* **57**(3): 606–607.
65. White, N.J., 2008. Qinghaosu (artemisinin): the price of success. *Science* **320**(5874): 330–334.
66. Wittig, R., Lohmann, J., Gmehling, J., 2003. Vapor-liquid equilibria by UNIFAC group contribution. 6. Revision and extension. *Ind. Eng. Chem. Res.* **42**(1): 183–188.
67. World Health Organisation, 2015. Q&A on artemisinin resistance. URL: http://www.who.int/malaria/media/artemisinin_resistance_qa/en/.
68. Wu, X., Deng, Z., Yan, J. et al., 2014. Experimental investigation on the solubility of oxygen in toluene and acetic acid. *Ind. Eng. Chem. Res.* **53**(23): 9932–9937.
69. Zhang, H., Lakerveld, R., Heider, P.L., Tao, M., Su, M. et al., 2014. Application of continuous crystallization in an integrated continuous pharmaceutical pilot plant. *Cryst. Growth Des.* **14**(5): 2148–2157.
70. Zhu, C., Cook, S.P., 2012. A concise synthesis of (+)–artemisinin. *J. Am. Chem. Soc.* **134**(33): 13577–13579.

APPENDIX

Solubility

The solubilities (saturation mole fractions, x_i^{sat}) of components in solvent mixtures are calculated using the following equation (Gracin et al., 2002):

$$a_i^s = x_i^{sat}\gamma_i^{sat} = \exp\left[\frac{\Delta H_{fus}}{R}\left(\frac{1}{T_{fus}} - \frac{1}{T}\right)\right] \tag{A1}$$

H_{fus} is the enthalpy of fusion and T_{fus} is pure solid solute *i* melting point. Solid activity (a_i^s) is first estimated via the exponential portion of Eq. (A1). Activity coefficient γ_i^{sat} is obtained from Eq. (A2) when then allows the calculation of x_i^{sat} via Eq. (A1). An iterative process is required for Eq. (A1), as the activity coefficient γ_i^{sat} also depends on mole fraction x_i^{sat}.

In the UNIFAC method the activity coefficient for molecule *i* (γ_i) is the sum of a combinatorial and residual components γ_i^c and γ_i^r , respectively (Fredenslund et al., 1975):

$$\ln \gamma_i = \ln \gamma_i^c + \ln \gamma_i^r \tag{A2}$$

The UNIQUAC model is used to compute γ_i^c (Abrams and Prausnitz, 1975):

$$\ln \gamma_i^c = \ln \frac{\phi_i}{x_i} + \frac{z}{2} q_i \ln \frac{\theta_i}{\phi_i} + L_i - \frac{\phi}{x_i}\sum_j x_j L_J \tag{A3}$$

In equation A2 ϕ_i is the molar weighted segment fractional component and θ_i is the area fractional component:

$$\phi_i = \frac{x_i r_i}{\sum_j x_j r_j} \tag{A4}$$

$$\theta_i = \frac{x_i q_i}{\sum_j x_j q_j} \tag{A5}$$

The UNIFAC compound parameter L_i is defined by r_i , q_i and *z*:

$$L_i = \frac{z}{2}(r_i - q_i) - (r_i - 1), \quad (z = 10) \tag{A6}$$

Parameters r_i and q_i , also used in computing ϕ_i θ_i, are calculated from volume (R) and surface area (Q) parameter contributions from functional groups:

$$r_i = \sum_k \nu_k^{(i)} R_k \tag{A7}$$

$$q_i = \sum_k \nu_k^{(i)} Q_k \tag{A8}$$

where ν_k is the number of occurrences of group k on a molecule.

The residual component γ_i^r is calculated from Γ_k and $\Gamma_k^{(i)}$, the residual group activity coefficient of group *k* in reality and in a reference solution of pure substance *i*, respectively:

$$\ln \gamma_i^r = \sum_k \nu_k^{(i)} \left[\ln \Gamma_k - \ln \Gamma_k^{(i)}\right] \tag{A9}$$

Both Γ_k and $\Gamma_k^{(i)}$ are calculated via the following equation:

$$\ln \Gamma_k = Q_k \left[1 - \ln \sum_m \theta_m \psi_{mk} - \sum_m \frac{\theta_m \psi_{km}}{\sum_n \theta_m \psi_{nm}} \right] \tag{A10}$$

where parameters θ_m and x_m (summation of the area fraction of group *m* over all different groups, and the mole fraction of group *m*, respectively) are defined as follows:

$$\theta_m = \frac{Q_m x_m}{\sum_n Q_n x_n} \tag{A11}$$

$$x_m = \frac{\sum_j \nu_m^j x_j}{\sum_j \sum_n \nu_n^j x_j} \tag{A12}$$

A modified Arrhenius equation is used to calculate Ψ_{mn} (a measure of interaction energy between groups):

$$\Psi_{mn} = \exp\left[-\frac{U_{mn} - U_{nm}}{RT} \right] \tag{A13}$$

Tables for group interactions and other parameters are widely available in literature (Wittig et al., 2003).